Electrochemically Tunable PEDOT:PSS Film for Surface Acoustic Wave-Based Humidity Sensing

Nour Abdallah, Alexandre Westrelin, Pierre Debavelaere, Mathieu Lefebvre, Olivier Stienne, Bilel Hafsi

Electrochemically Tunable PEDOT:PSS Film for Surface Acoustic Wave-Based Humidity Sensing

N. Abdallah[1,2*], A.Westrelin[1], P. Debaveleare[2], M. Lefebvre[2], O.Stienne[2], B. Hafsi[1,2*]

[1] Univ. Lille, CNRS, Centrale Lille, Univ. Polytechnique Hauts-de-France, UMR 8520 - IEMN, F-59000 Lille, France.
[2] Icam School of Engineering, 06 rue Auber, 59800, Lille, France

Corresponding authors: Nour.Abdallah@icam.fr / bilel.hafsi@icam.fr

Abstract— The increasing demand for humidity detection in both commercial and industrial applications has driven the rapid advancement of humidity sensors built on various technologies. Among these, surface acoustic wave (SAW) technology has emerged as a promising solution, thanks to its inherent advantages, including compact size, high sensitivity, and straightforward operating principle. In this study, we present a surface acoustic wave (SAW)-based humidity sensor featuring a functional polymer film as the active sensing layer. The film was deposited through an electrochemical bottom-up approach using the monomer 3,4-ethylenedioxythiophene (EDOT) and the polyelectrolyte Poly(sodium 4-styrenesulfonate) (PSS) in deionized water. Cyclic voltammetry was employed to optimize the deposition process, ensuring controlled film growth and a preserved radiofrequency response of the sensor. The resulting PEDOT:PSS film was extensively characterized morphologically via Optical Microscopy and Atomic Force Microscopy (AFM). Sensor's electrical properties were assessed using a Vector Network Analyzer (VNA) under controlled environment. The sensor exhibits a maximum sensitivity of 16.8 ppm/%RH and a detection limit (LOD) of 0.3 %RH. The study further explores the enhancement of humidity sensitivity through the active layer surface control, aiming to improve sorption interactions and selectivity. These findings contribute to the development of high-performance SAW humidity sensors with potential for integration into compact, low-power monitoring systems.

Keywords— PEDOT:PSS, Electropolymerization, Humidity sensing, Surface acoustic wave (SAW), Organic sensors.

I. INTRODUCTION

Humidity is a critical environmental factor that significantly affects numerous areas of everyday life. Beyond ensuring human comfort, accurate monitoring and control of humidity are essential in various manufacturing and storage settings to maintain optimal production quality [1], [2], [3].

Current research on humidity sensors primarily focuses on optical [4], resistive [5], capacitive [6], and acoustic resonator-based devices [7], [8]. While capacitive and resistive sensors offer advantages such as compact size, simplicity, and low cost, they are often limited by low measurement accuracy. Impedance-based humidity sensors, while widely used, present several limitations. Their performance is often affected by temperature variations and frequency dependence, leading to reduced accuracy without proper compensation.

On the other hand, acoustic resonator-based sensors, especially those whose function depend on surface acoustic waves, offer several advantages, including compact size, high sensitivity [9], [10], straightforward fabrication, and excellent measurement stability over a wide range of operating conditions. Using ST-cut quartz as the piezoelectric substrate provides excellent temperature stability, low acoustic loss, and compatibility with well-established high-precision microfabrication techniques. These characteristics make quartz particularly suitable for reliable and repeatable SAW device performance in sensing applications. Beyond the sensing technology itself, selecting appropriate humidity-sensitive materials is essential for developing high-performance humidity sensors. Commonly used active layer materials include ceramics [11], metal oxides [12], 2D materials [13], and conducting polymers (CPs) [14] . Among the latter, the poly(3,4-ethylenedioxythiophene) polystyrene sulfonate (PEDOT:PSS) has recently attracted considerable attention [15] [16]. Drawing upon its distinctive molecular structure rendering it highly hygroscopic [17], PEDOT:PSS has been widely employed as an active layer in humidity sensing devices reported in literature [18], [19], [20].

Similar to other CPs [21] [22], the functionalization process of PEDOT:PSS film may adopt many configurations, primarily involving depositing the polymeric solution or in situ polymerization of the monomer. For polymer solution-based deposition, reported techniques include drop-casting [23], inkjet printing [24], spin coating [25], electrospinning [26] [27], and dip coating [28]. On the other hand, fabrication based on monomer solutions requires oxidative polymerization, which can be homogeneous (chemically initiated) or heterogeneous (electrically initiated). Both methods benefit from EDOT's high oxidative potential, which is in turn devoted to the ethylenedioxy bridge increasing the electron density on the thiophene ring, and the lower band gap of the conjugated polymer [29]. Homogeneous polymerization offers simple and fast processes, however, it cannot achieve strong polymer adhesion and precise control over film thickness and morphology [30]. Indeed, this can be achieved by heterogeneous polymerization through techniques like cyclic voltammetry, in which these properties can be precisely tuned by adjusting parameters like the scan rate, potential range, and number of cycles. Such polymeric properties are also widely dependent over the electrolyte nature [31], temperature [32], PH [33], and solvent [34].

In this work, we demonstrated a highly sensitive and tunable humidity sensor based single-port SAW resonator. Fabricated on piezoelectric ST-Quartz material, interdigital transducer (IDT) electrodes were modified by means of PDOT:PSS electropolymerization. Cyclic voltammetry was employed to optimize the deposition process, ensuring uniform film growth and desirable electrochemical properties. To analyze the electrical behavior of the SAW resonator, we developed a modified Butterworth–Van Dyke (mBVD) equivalent-circuit model implemented in Python. The performances of the proposed SAW humidity sensors were investigated systematically, including their sensitivity, reproducibility, sensing mechanism, repeatability, response, and recovery time.

II. MATERIALS AND METHODS

A. Materials

3,4-Ethylenedioxythiophene (EDOT, ≥97%) and sodium polystyrene sulfonate (PSSNa, Mw ≈ 70,000), both purchased from by Sigma-Aldrich, were used without further purification. Sensors were made on ST-cut quartz substrates (Precision Micro-Optics Inc.), commonly employed for surface acoustic wave (SAW). Deionized water (DI) was used throughout the preparation of all aqueous solutions and for rinsing steps to prevent any ionic contamination that could affect the electrochemical polymerization process. A high-purity nitrogen cylinder was used as the carrier gas during humidity experiments, providing a controlled environment.

B. Methods

SAW Sensors Design and Fabrication: A 4-inch ST-cut quartz wafer with a single side polished was used as the piezoelectric substrate in this work. The wafer was cleaned by sonication in acetone, isopropanol, for 15 min in each solvent, followed by ultraviolet irradiation in an ozone atmosphere (ozonolysis) for 30 min to eliminate dust and contaminants from the substrate's surface. Following the cleaning process, the substrate was dried with high-purity nitrogen gas.

Table 1. Design parameters of SAW devices

Construction parameters
Working Frequency = [431.7 - 436.6] MHz
Metal Thickness: (Ti/Au)=(10nm/100nm)
Reflector Qty: Nbr= 4
Transducer Fingers: NP= 50
Reflector Fingers: Nr= 16
Separation: Lg= λ/4
Gap= 1 λ
Root= 4λ
Metallization ratio= 0.5
Material parameters
Material: Quartz
Orientation: ST-Cut (+42.75Y)
Free velocity: V=5100 $m.s^{-1}$
Wave velocity : v=4475 $m.s^{-1}$

The cleaned substrate was subsequently coated with a positive photoresist bilayer (COPO El 13% / PMMA). After the e-beam lithography process, the bilayer photoresist was developed in MIBK (methyl isobutyl ketone) and IPA (isopropyl alcohol) for 30s. A (Ti/Au) IDT electrodes, used to construct SAW devices, were then thermally evaporated on top of the substrate. Finally, a lift-off process was conducted by immersing in organic solvent (SVC-14) at 70°C for 2h, followed by rinsing in acetone and IPA, and drying with nitrogen. The device comprises a set of reflector gratings that form an acoustic cavity, along with an Interdigital Transducer (IDT) that couples acoustic energy into this cavity. The device consists of 50 interdigitated gold fingers that are 2.58 µm wide and 110 nm thick, Fig.**1a**. The device supports the propagation of shear-horizontal surface acoustic waves (SH-SAWs).To improve the electrical performance of the studied resonators, several fabrication parameters were optimized **[35]**, including the number of IDT finger pairs (Np), finger width (W), number of reflector electrodes (Nr), and number of Bragg reflectors (Nbr) . The corresponding material properties and design specifications of the SAW resonator studied in this paper are summarized in Table **1**. The sensing surface of the resonator is functionalized using a bottom-up growth of a conducting polymer (PEDOT:PSS) **[36]**, via electropolymerization method, employing a three electrodes system, Fig. **1b**.

When exposed to water vapor, the modified SAW sensor undergoes mass loading due to the adsorption of water molecules. This interaction alters both the velocity and amplitude of the SH acoustic waves propagating through the device. The change in acoustic wave velocity can be expressed by the following *equation* **[37]**, assuming that the variation in substrate elasticity is negligible.

$$\frac{\delta V}{V_0} = -\frac{V_0^2}{4}\left(\frac{2\pi}{\lambda}\cdot A\right)\delta\rho \qquad (1)$$

Where $\delta V/V_0$ represents the relative change in the SAW phase velocity, $\delta\rho$ is the variation in mass density, λ is the acoustic wavelength, and A corresponds to the mechanical displacement within the SAW sensor structure.

Solution Preparation: Aqueous solution of EDOT(10 mM) and PSS(10mM) were prepared in a clean room. To solubilize EDOT by means of PSS emulsions, further heating and mixing were done using an ultrasonic water bath for less than 5 minutes.

Electrodeposition: Before and after each polymerization process, the sensors were rinsed with DI water and dried with an air stream. The experimental setup consisted of a three-electrode configuration comprising a gold working electrode (WE), a platinum counter electrode (CE), and an Ag/AgCl-coated silver wire serving as the reference electrode (RE), as shown in Fig. **1b.** The RE was injected into the well through a pierced hole to maintain the proper surface area ratio and spatial positioning relative to the counter electrode (CE), in accordance with electrochemical cell requirements.

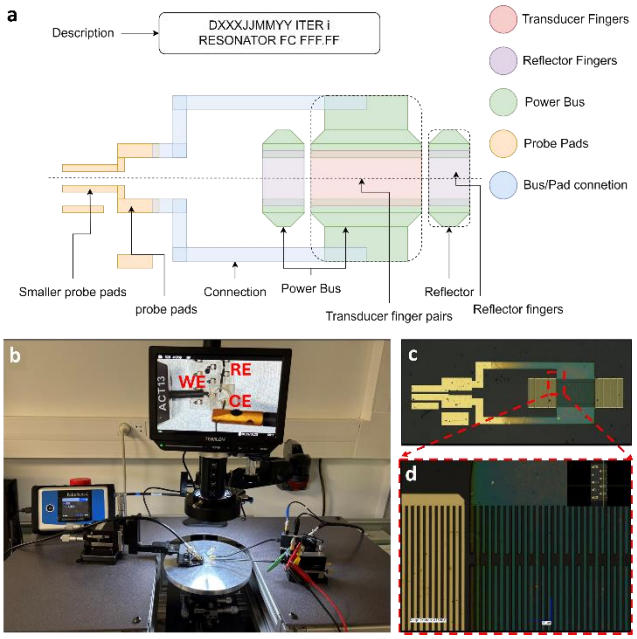

Fig.1. (a) Design parameters of a one-port SAW resonator (b) electrochemical setup showing the working, reference and counter electrodes embedded into the PDMS well. (c) Optical microscopy images of the functionalized SAW (d) Zoom on IDT fingers.

For each electropolymerization experiment, 30µl of the solution is inserted into a PDMS well on top of the printed working electrode. A Palmsens 4 potentiostat/galvanostat was employed to control and monitor the electrochemical parameters. This setup ensured uniform polymer growth and a quasi-reproducible film characteristics across all fabricated samples. Electrochemical measurements were carried out at room temperature under varying applied potentials, scan rates, and numbers of cycles. Figures **1.c** and **1.d** present the selectively electropolymerized IDTs of the SAW resonator.

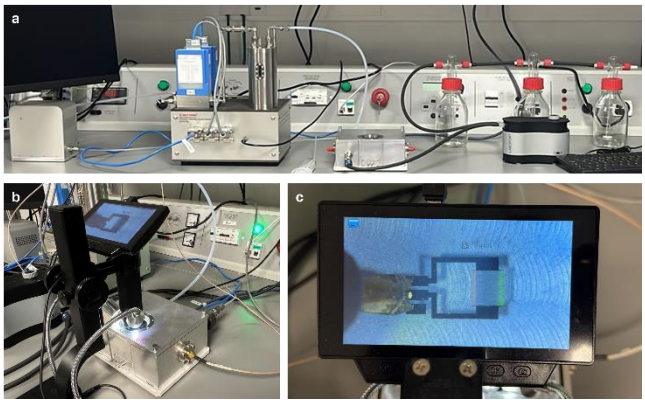

Fig. 2. Humidity sensing measurement set up.

Humidity Sensing Setup: The humidity sensing characterization setup is illustrated in Fig.**2**. The SAW humidity sensor was mounted inside a sealed measurement chamber connected to a Nextron Micro Probe System, which supports precise environmental control. The Relative humidity (RH) within the chamber was controlled using a precision humidity regulation system composed of a dual-channel mass flow controller (MFC), a 200 cc deionized (DI) water bubbling bath, and dedicated PID-based humidity control software. This system enables fast and accurate modulation of RH from 4% to 95%, with a typical ramp speed of 10% RH per minute, an accuracy of ±2% RH, and a resolution of 0.1% RH. Nitrogen (N_2) was used as the carrier gas during the measurements, with a total flow rate maintained at 500 SCCM.

Radiofrequency characterization: Electrical characterization of the fabricated SAW devices under controlled humidity conditions was conducted using a calibrated Rohde & Schwarz Vector Network Analyzer (VNA) operating across the 9 kHz to 6 GHz range. The VNA was connected to the sensor via precision micro-probes in the Nextron system. Scattering parameters (S-parameters) were recorded for each sensor to evaluate key electrical performance metrics, including resonance frequency shift, quality factor, electromechanical coupling coefficient and impedance matching.

III. RESULTS AND DISCUSSION

A. EDOT:PSS Electropolymerization on SAW resonator

To ensure a uniform film growth and preserve the acoustic performance of the device, cyclic voltammetry was employed. We first started by setting a wide voltage scan range to initiate the electropolymerization process. The voltammogram obtained is shown in Fig.**3.a** and it reveals a quasi-reversible electrochemical behavior of EDOT:PSS solution within a potential window of [-1V, 1V]. First, the monomer is oxidized showing a pronounced anodic peak at 1V, leading to PEDOT:PSS polymer formation. Then, with the reverse sweeping, the bipolaronic and polaronic neutralization of PEDOT+ occurs, as observed by the presence of two small reduction peaks respectively around -0.499 V and -0.8 V **[38]**. Another confirmation of EDOT polymerization is given by the nucleation loop formation during the oxidation phase of the first cycle, which is another characteristic feature for polymer initiation and growth **[39].**

Subsequent experiments were performed within a narrower potential window, with the minimum reduction potential limited to -0.5V, Fig. **3.b**. This adjustment improves the mechanical stability of PEDOT polymer by limiting its reduction on the gold surface. At lower reduction potentials, $PEDOT^+$ becomes de-doped into its neutral state, thereby weakening its interactions with PSS anions. Consequently, hydrogen bonding between PSS and water molecules is favored. During cycling, the repeated transition between the de-doped (swollen) and doped (contracted) states of PEDOT in backward and forward sweeps ultimately degrades the polymer's mechanical properties over time. Limiting the reduction potential also helps shorten the electropolymerization duration, resulting in improved process repeatability and more uniform film formation.

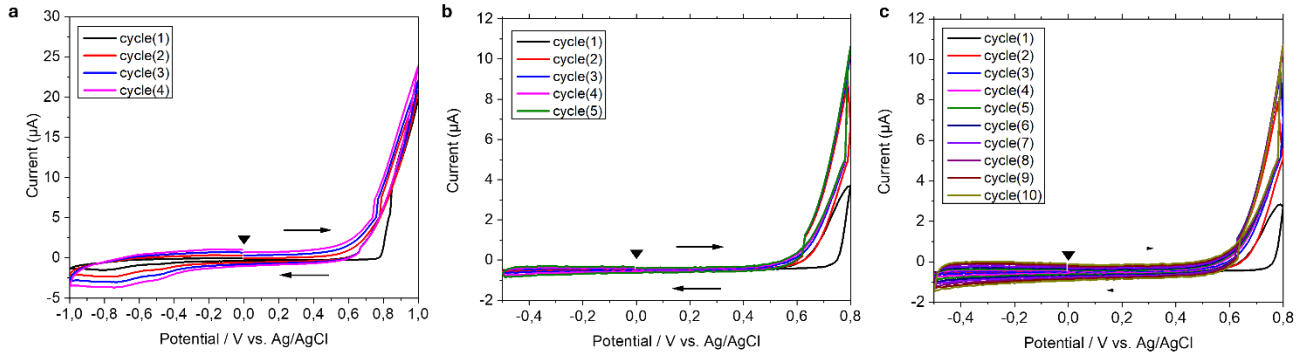

Fig.3. Cyclic Voltammograms corresponding to the electropolymerization of EDOT:PSS at v= 100 mV/s in the potential window a) [-1, 1V] & 4 cycles, b)) [-0.5,0.8V] & 5 cycles and c) [-0.5,0.8V] &10 cycles.

To further investigate the capacitive behavior that may occur during the electropolymerization process, two voltammograms were recorded and presented in Fig. **3.b** and **3.c**. Both voltammograms illustrate the electropolymerization of EDOT:PSS within a potential window of [−0.5 V, 0.8 V], performed over 5 and 10 cycles, respectively. Notably, distinct capacitive behavior emerges only when polymerizing EDOT:PSS for more than 3 cycles (Fig. **3.c**). This was also seen with other potential windows (see supplementary information Fig. **S1**). Such a phenomenon is likely attributed to charge accumulation at the electrode-polymer interface. Hence, during the electrochemical deposition of PEDOT:PSS, part of the applied charge is stored within the electric double layer that forms at the interface between the film and the electrode surface.

B. Optimization of the Electropolymerization Process

Through this work, we proceeded to understand the CV parameters' control over EDOT polymerization rate, and PEDOT:PSS thickness and morphology. For this, we investigated the effects of the scan rate, the cycling potential window, and the number of cycles.

a. *Scan Rate Effect*

EDOT:PSS was electropolymerized onto four distinct SAW resonators, precisely covering the active regions of the interdigital transducers (IDTs). Each device was subjected to four cycles within a potential window of −0.5 V to 0.8 V, and at different scan rates: 25, 50, 100, and 200 mV.s^{-1} (Fig.**4**). The analysis of the obtained CV-curves is crucial for understanding the dominant mechanism governing the electropolymerization reaction. Accordingly, the Randles–Ševčík approach was applied to assess the kinetic behavior of the process (see Supplementary Information). In fact, the two box plots of Fig.**S5** show a very low correlation factor R^2 ~0.141 and 0.109, proving that the electrochemical behavior of the monomeric solution is controlled by both EDOT diffusion and PEDOT growth onto the gold electrode.

Optical images of the polymerized SAW devices are depicted in Fig.**4**. It is clear that the Bragg reflectors remain unmodified during the electropolymerization process, retaining their characteristic gold appearance. This further highlights the localized and well-confined polymer growth over the IDTs region.

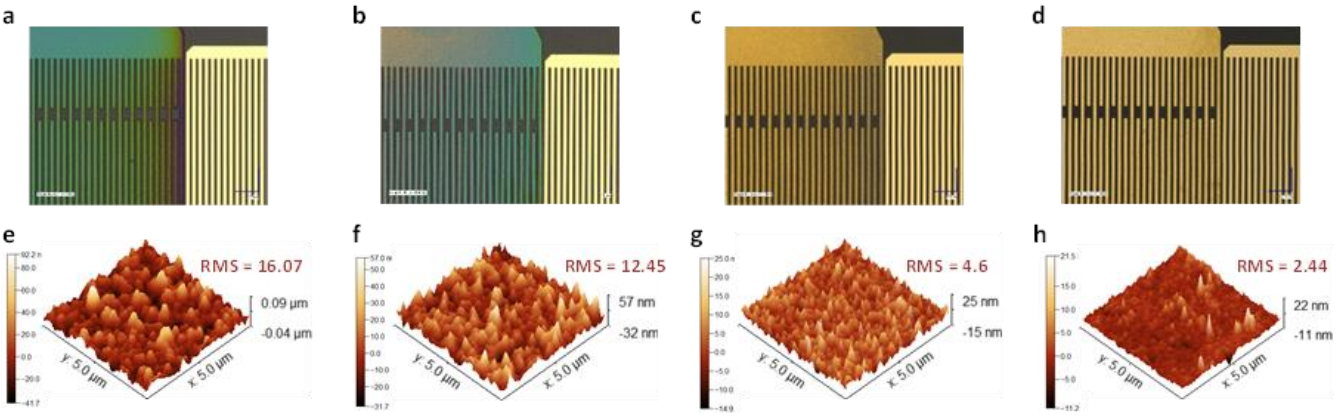

Fig.4. Morphological characterization: Optical Microscopy images (a-d) and the corresponding Atomic Force Microscopy images (e-h) of polymerized SAW devices within a potential window [-0.5V, 0.8V] based on 4 cycles at different scan rates (a, e) 25 mV.s^{-1}, (b, f) 50 mV.s^{-1}, (c, g) 100 mV.s^{-1}, and (d, h) 200 mV

On the other hand, the color contrast of PEDOT:PSS films on the interdigitated fingers fades progressively as the scan rate increases from 25 to 200 mV.s^{-1} (Fig.4a–d), indicating a reduction in the polymer film thickness and surface coverage. This observation is further supported by the profilometry measurements summarized in Table 2, which show a consistent decreasing trend in film thickness with increasing scan rates. For instance, the highest polymer thickness (~243 ± 14 nm) was obtained for devices electropolymerized at 25 mV.s^{-1}, whereas those processed at 200 mV.s^{-1} exhibited a significantly thinner layer of 22 ± 4 nm. To confirm these findings, complementary AFM characterization (Fig.4e–h) was performed, revealing a progressive decrease in both height and surface roughness. This confirms the formation of thinner and more compact PEDOT:PSS layers at higher scan rates.

Table 2. Profilometry results revealing the polymer thicknesses on different SAW devices electropolymerized within [-0.5, 0.8V] with 4 cycles at different scan rates

Scan rate mV.s^{-1}	Thickness (nm)
25	*243 ±14*
50	*134 ±29*
100	*72 ± 16*
200	*22 ± 4*

For instance, the root mean square roughness (RMS) of the film has successively decreased from 16.07 to 2.44 over increasing the scan rate from 25 to 200 mV.s^{-1}. At higher scan rates, the potential sweep becomes too fast for EDOT monomers to diffuse efficiently to the electrode surface, and the rate of electron transfer may surpass that of analyte diffusion. This results in a lower concentration of oxidized EDOT radical cations available for the polymerization. Not only can this explain the variations in the thickness parameter, as fewer PEDOT polymers are consequently synthesized, but it can also account for the changes in surface roughness, which is highly dependent on PEDOT chain length that becomes shorter at higher scan rates.

b. Potential Window / number of cycles Effect

To assess the effect of the potential window and number of cycles on the electropolymerization process, we specifically focus on key outcomes such as polymer thickness, morphology, and the mass influence on the electrical characteristics of our devices. Our study was conducted by electropolymerizing EDOT:PSS at a fixed scan rate of 100 mV.s^{-1}, with a constant minimum reduction potential of -0.5V, while varying the maximum oxidation potential from 0.75V to 1V. For each case, the influence of the number of cycles was also examined by performing 6, 8, and 10 polymerization cycles. The quantification of polymer deposition was based on the charge exchanges on the working electrode surface which were extracted following *equation* 2, [40]:

$$Qc = \int i(t) \times dt = \int_{n=1}^{N} i(n) \times \Delta t = \int_{n=1}^{N} i(n) \times 2 \frac{V_{max} - V_{min}}{scan\ rate} \times \frac{number\ of\ cycles}{number\ of\ data\ points} \quad (2)$$

Calculated charge values are summarized in the plot presented in Fig.5a. For all devices electropolymerized with the same number of cycles along with the increase of maximum potential, the plot shows a proportional increase in the average charge currents. For example, during the electropolymerization of EDOT:PSS with a maximum oxidation potential of 0.75V, the recorded mean charge value was 25 µC. This value progressively increases to 80 µC, 277 µC, then 560 µC as the maximum oxidation potential is raised to 0.8V, 0.9V, and 1V respectively. Such a proportionality is preserved with all devices being electropolymerized with the other numbers of cycles. On the other hand, SAW devices electropolymerized at the same maximum oxidation potential but with different numbers of cycles did not exhibit a linear trend in the charge quantity. As a further analysis of the influence of these two parameters on PEDOT:PSS deposition, optical microscopy images were captured for these devices (Fig.5.b). In particular, these results reveal similar coloration of IDTs which are electropolymerized at the same maximum oxidation potential (e.g., 0.75V) and regardless of the cycling number (6 , 8, 10). Indeed, this shows similar polymer growth and confirms again the insignificant impact of the cycling number. Alternatively, the observations across different maximum oxidation potentials for a fixed number of cycles were unique. All devices with a maximum oxidation potential reaching 1V exhibit undesirable polymerization on the Bragg reflectors, suggesting an extensive 2-D horizontal growth of the polymer over the surface of the interdigitated fingers. This can be attributed to PEDOT's conductive nature and the local electric field effect. Besides, we can observe short-circuiting across the IDTs themselves for all devices electropolymerized at the oxidation potential of 0.9V and 1 V, and this occurs even with the lowest number of cycles during this experiment. As a result, once the polymer growth extends sufficiently to reach the gold reflectors, it causes a short circuit, effectively incorporating the reflectors into the electrical path and enabling further PEDOT polymerization on their surface. In fact, this increases the effective surface area for polymerization and can alter the expected thickness and mass of the deposited PEDOT layer. On the other hand, devices electropolymerized within the oxidation potentials of 0.75 V and 0.8 V showed no short-circuiting across the IDTs, even after 10 cycles. Moreover, the uniform coloration and absence of afore-noticed clusters indicate a more homogeneous polymer distribution.

To assess the impact of the deposited polymer on the electrical response of the sensor, we sought to identify an optimal potential that ensures sufficient polymer growth while preserving the acoustic and the electrical performances of the SAW resonators. For this, a systematic radiofrequency (RF) characterization was carried out using reflection scattering parameter (S_{11}) measurements following the electrodeposition

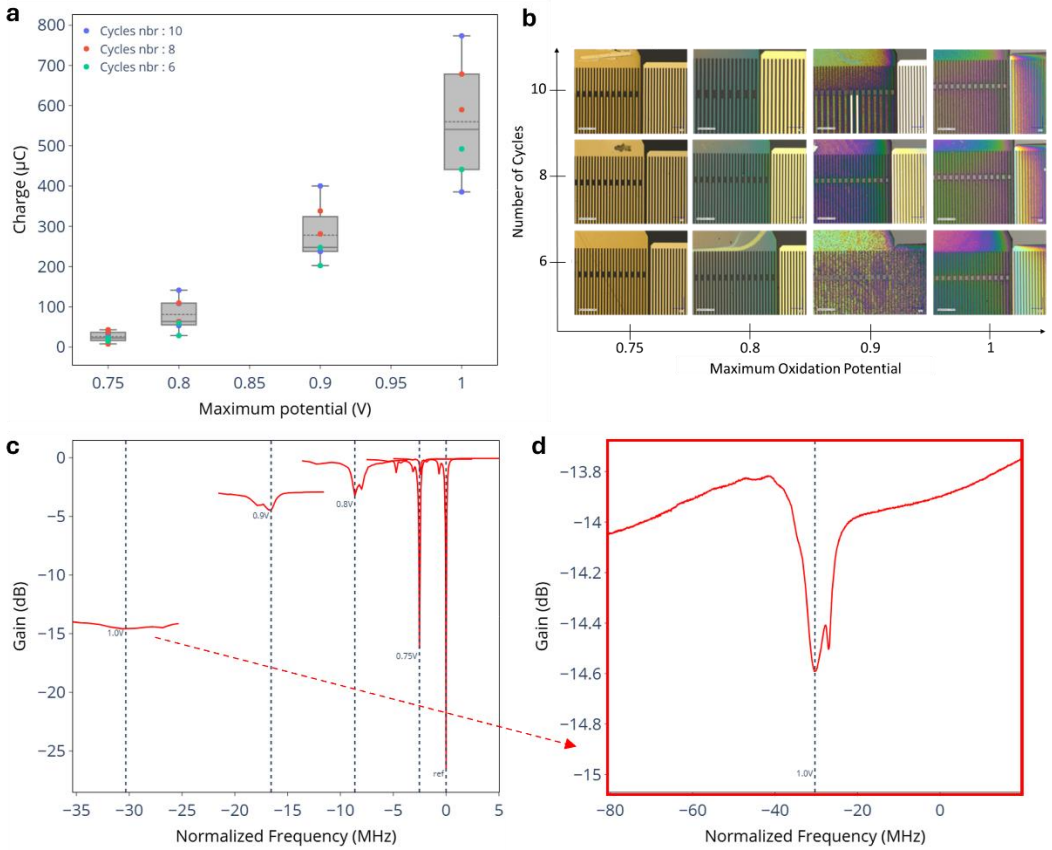

Fig. 5. a. Average peak current variations extracted from CV voltammogramme, b. the corresponding optical microscopy images of devices electropolymerized at v= 100 mV/s with different number of cycles and maximum oxidation potentials, c. Normalized S_{11} Gain response versus the applied oxidation potential E_1, d. Zoom normalized S_{11} Gain response for E_1=1V applied potential.

process. The data presented in Fig.5c-d indicates that increasing the oxidation potential leads to a gradual decrease in both the rejection level and the quality factor. Specifically, the rejection level decreases from −26.5 dB to −0.84 dB when the potential increases from 0.75 V to 1.0 V. The observed shift in the resonance frequency further indicates an increased mass loading effect associated with thicker polymer deposition. Based on these results, an optimal oxidation potential of E_1 = 0.75 V was identified, above which the RF performance of the devices begins to degrade.

C. Modified Butterworth-Van Dyke Equivalent Circuit

In order to investigate the impact of PEDOT:PSS growth on the surface acoustic wave (SAW) resonator, the reflection scattering parameter S_{11} was modeled using a modified Butterworth–Van Dyke (mBVD) equivalent circuit, Fig. 6a. This model was generalized in the whole humidity spectrum (see supporting information). In the fitting plots, the solid curve corresponds to the measured data, while the dashed curve represents the fitted response obtained from the mBVD model. Fig.6b and 6c show the scattering parameter (S_{11}) responses of both the unmodified SAW resonator and the PEDOT:PSS-modified device, respectively. The resonant frequency (f_r), anti-resonant (f_a) frequency and Conductance Full Width at Half Modulation (GFWHM), were extracted from Conductance (G) and Impedance (Z) measurements. The resonator's quality factor (Q) and the electromechanical coupling coefficient (K^2) were then extracted using equations 3 and 4.

$$Q = \frac{f_r}{G_{FWHM}} \tag{3}$$

$$K^2 = \frac{\pi}{2} \times \frac{f_r}{f_a} \times \tan\left(\frac{\pi}{2} \times \frac{f_a - f_r}{f_a}\right) \tag{4}$$

After functionalization, key circuit parameters were extracted from the fitted mBVD model. The reference SAW resonator exhibits a resonance frequency of 436.580 MHz, a return loss of −27.25 dB, and a quality factor (Q) of 3830. After PEDOT:PSS deposition, the resonance frequency shifts to 431.82 MHz, with a return loss of −11.33 dB and a reduced Q factor of 2601. This frequency downshift of approximately 4.66 MHz is attributed to the mass loading effect induced by the PEDOT:PSS layer. The electropolymerized polymer causes a degradation in return loss, which further contributes to the decrease in the Q factor. A comparison of the SAW resonator parameters before and after electropolymerization with PEDOT:PSS is presented in Table 3. The results show that the motional resistance (R_m) increased substantially from 54.44 Ω to 98.93 Ω, reflecting higher acoustic losses after polymer electrodeposition.

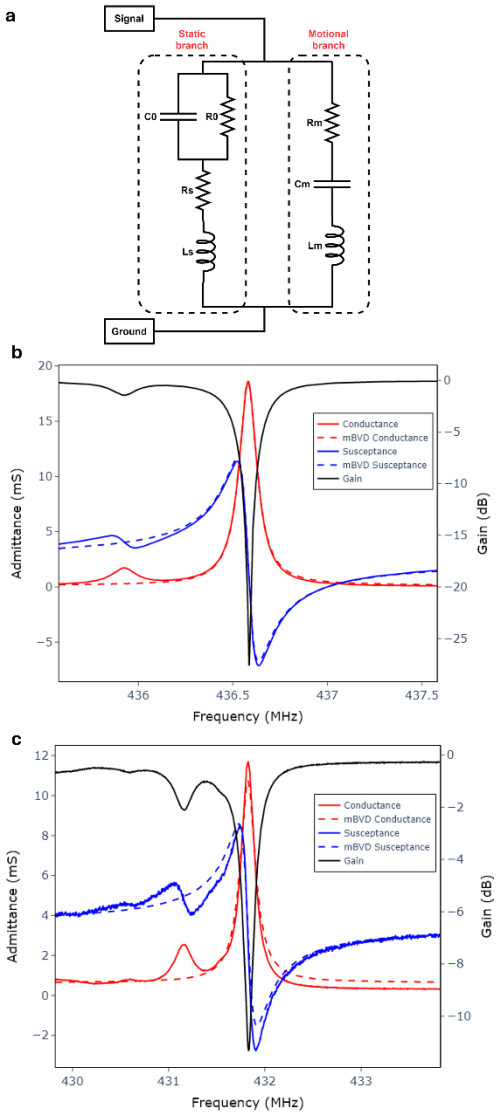

Fig. 6. a. Modified Butterworth von Dyke model divided in a real capacitor model and a piezoelectric-induced motional branch. Scattering parameter S11 variation with frequency : b. reference SAW resonator, c. PEDOT:PSS modified SAW resonator

In our model, this motional resistance is governed by a quadratic equation depicting the non-linearity of the amplitude. The motional inductance (L_m) exhibits a slight increase from 76 µH to 82 µH, while the motional capacitance (C_m) decreases marginally from 1.8 fF to 1.65 fF. These parameters are the primary factors that determine the resonant frequency. Because of its geometry and the nature of the substrate, the IDT of the SAW resonator exhibits a capacitive behaviour. This effect is represented in our mBVD model by the static branch, characterized by the capacitance C_0, which increases from 0.89 pF to 1.32 pF. The variation in C_0 can be attributed to the standard capacitive behaviour of the IDT structure. Considering the fabrication characteristics of the sensor, the IDT geometry effectively forms a parallel-plate capacitor. According to the classical capacitance relation:

$$C = \varepsilon_r \frac{S}{D} \quad (5)$$

where ε_r is the relative permittivity of the medium, S is the effective electrode's surface area and D is the separation between electrodes.

Table 3. mBVD model parameters

Parameters	Reference SAW	PEDOT :PSS SAW
R_m	54.44 Ω	98.93 Ω
L_m	76.23 µH	82.6 µH
C_m	1.8 fF	1.65 fF
C_0	0.89 pF	1.32 pF
R_0	11.38 KΩ	2.65 KΩ
R_s	8.75 Ω	21.2 Ω
L_s	491.12 pH	671.65 pH
Q	3830	2601
Q_{mBVD}	3830	2249
K^2	2.39 ‰	1.69 ‰
K^2_{mBVD}	2.43 ‰	1.65 ‰
R^2	99.01 %	94.89 %
f_r	436.58 MHz	431.82 MHz
D	2.548 µm	2.510 µm

Based on AFM images we can measure the variation in finger width (D). From the data in Table 3 it can be seen that the effective surface area increased by 46%, which explains the C_0 variation. Furthermore, the IDT capacitor, at these working frequencies, exhibits parasitic elements that cannot be neglected and especially after polymerization. This behaviour can be represented by a leakage resistor (R_0) decreasing from 11.38 kΩ to 2.65 kΩ, a resistor (R_s) increasing from 8.75 Ω to 21.2 Ω, and an inductor (L_s) which increase from 491.12 pH to 671.65 pH. We should note that regarding all static branch parameters, R_s exhibits a clear dependence toward humidity, reflecting humidity-induced modifications in the electrical properties of the PEDOT:PSS layer. This tends to indicate a sub-skin depth Metallo-organic interface mechanism underlying the humidity dependent semiconductor behavior [41].

D. Humidity Sensing Results

The sensing performance of the fabricated SAW devices was studied by humidity characterization experiments. Measurements were carried out over a wide %RH range (from 10% to 80%) using a precision humidity control setup described in section II.

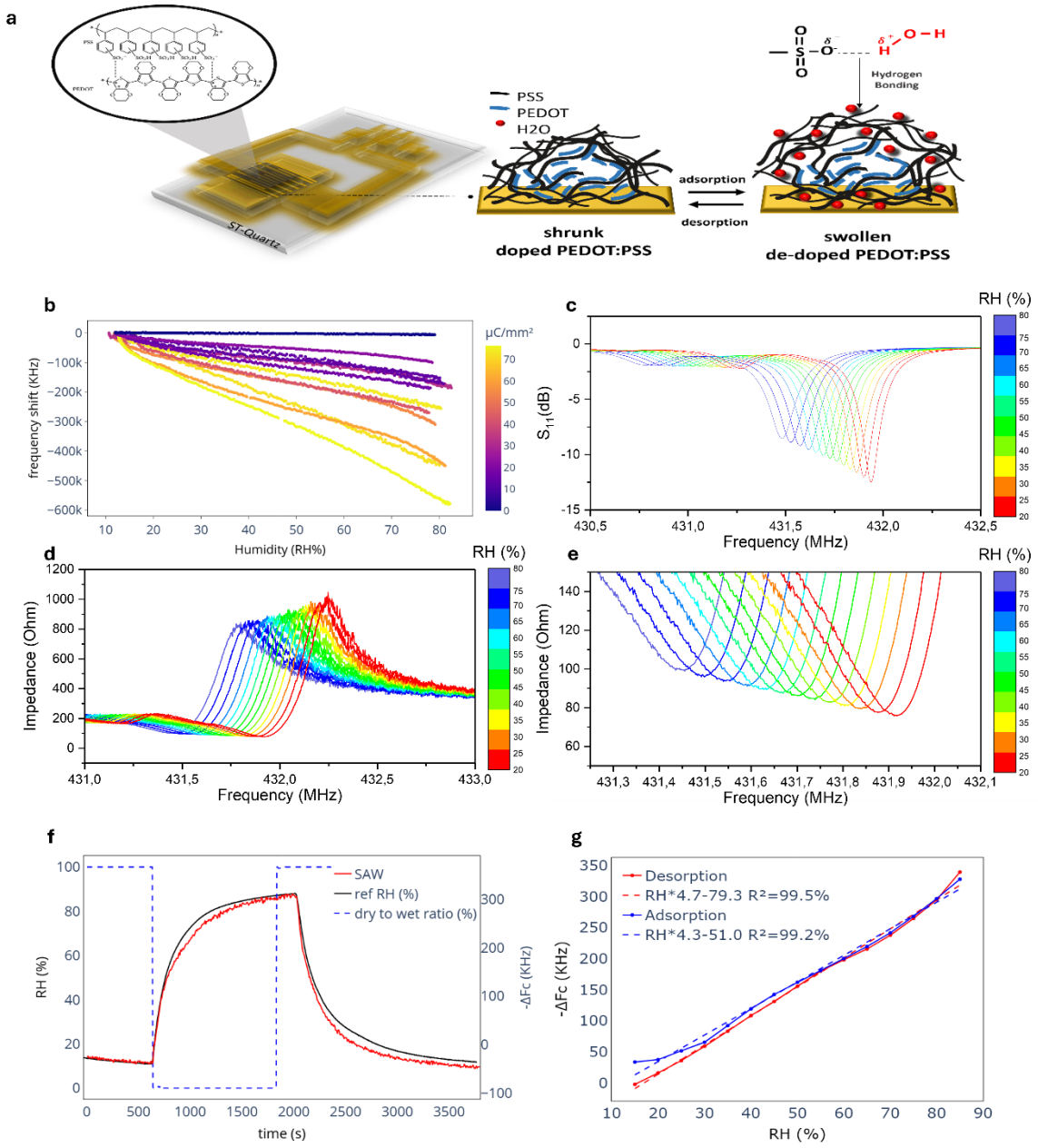

Fig. 7. (a). illustration of the mechanical effect of water interaction with PEDOT:PSS sensing layer. (b) frequency shift Δf versus relative humidity %RH for distinct recorded charge densities, (c-g) Dynamic responses of the selected SAW sensor (with charge density of 76 µC/mm^2) versus the humidity variations (%RH): (c) Reflection scattering parameter S_{11} amplitude (dB), (d) Impedance variation, (e) Zoom on impedance values at the resonance frequency, (f) Transient response of the resonator (red curve) vs. the humidity sensor of the Nextron system (black curve), (g) Hysteresis characteristics of the SAW sensor.

The aim of this study is to assess the response of the PEDOT:PSS-modified resonators to relative humidity (%RH) variations and to correlate these responses with the film's electrochemical properties. The importance of this correlation lies in the dependence of the polymer's mass on the overall charge density transfer during electropolymerization. The sensing mechanism is governed by a decrease in the SAW resonator's resonant frequency, which occurs as water molecules are adsorbed into the PEDOT:PSS layer. This frequency shift occurs primarily from the mass loading effect, where the adsorbed water molecules increase the effective mass on the active surface, thereby reducing the acoustic wave velocity. Additionally, the absorbed moisture alters the dielectric constant and conductivity of the PEDOT:PSS film, producing an electrical loading effect that further influences the propagation of surface acoustic waves. The interaction between PEDOT:PSS and water molecules (Fig. 7a) arises from both hydrogen bonding and electrostatic attraction between the negatively charged sulfonate ($–SO_3^-$) groups of PSS and the partial positive charge of water molecules [42], [43]. These interactions contribute to reversible water adsorption on the polymer surface, resulting in measurable shifts in resonant frequency and signal amplitude. This behavior was further examined through quantitative analysis.

The frequency responses of modified-SAW sensors were analyzed under different humidity levels. Fig.7b shows the frequency shift (Δf) observed as a function of the charge density obtained from the different electrochemical depositions. The curves reveal a proportional relationship between the increase in frequency shift and the increase in charge density. A maximum shift of 562 kHz is reached at a relative humidity (RH) level of 80%, with a sensor marking a charge density of approximately 76 µC/mm² during electropolymerization. This selected sensor has thus constituted the focus of our next studies shown in Fig. 7c-g. We first extracted the reflection characteristics (S_{11}) as shown in Fig.7c. Indeed, when the sensor is subjected to variations in relative humidity from 25%RH to 80%RH, the resonance frequency shifts toward lower frequencies, accompanied by a decrease in the amplitude of the S_{11} reflection signal. Fig.7d-e illustrate the variation in input impedance of the SAW resonator, presenting the maximum shift, under the same conditions. At 20% RH, the series resonant frequency (f_r) of the resonator is measured to be 431,91 MHz, with a corresponding series input impedance (Z_r) of 75.70 Ω. As the humidity increases to 55% RH, fr shifts downward to 431,67 MHz, while Z_r rises to 87.65 Ω. This trend continues with increasing humidity, showing a clear correlation between higher RH and both a decrease in resonant frequency and an increase in input impedance. At the highest tested humidity level of 80% RH, the resonant frequency shifts to 431.44 kHz, and the series input impedance increases to 99.52 Ω. These changes are primarily attributed to the swelling behavior of the deposited PEDOT:PSS film under humid conditions.

These observations can be described with reliance on the underlying interactions between water molecules and the polymeric layer. Specifically, water molecules, via the partial positive charge on hydrogen atoms, interacts with the negatively charged sulfonate ($–SO_3^-$) groups of PSS^- (fig.7.a). As the relative humidity increases, the surface mass of PEDOT:PSS increases. This swelling effect contributes to the observed downshift in resonant frequency and can explain the previously discussed results of figures 7.b and 7.c.

During both adsorption and desorption phases, the accuracy of the previous results was verified by comparing humidity levels detected by the resonator to those of the humidity sensor of the Nextron system (Fig. 7). For both phases, humidity was tested in the range of 15% to 80% RH. Given the grain-like structure of the polymer described by Saha *et al*. [44], this volumetric expansion of PSS-rich shell increases the space between adjacent PEDOT polymers reducing thus their pi interactions. This creates a drop in the transfer of positive charge carriers (holes) which in turn lessens the polymer's conductivity and rises the input impedance [16].

The reversibility of the water adsorption mechanism is indeed crucial for sensing applications in terms of sensor's recyclability. For this, hysteresis test was performed on the PEDOT:PSS-coated SAW humidity sensor and the results are shown in Fig. 7g. Inside the test chamber, the device was cycled from 15% RH up to 85% RH, and then back to 15% RH. The hysteresis remains minimal for RH values above 25%, with the adsorption–desorption gap limited to less than 11 kHz, highlighting the sensor's excellent reversibility. Linear regression analysis of the adsorption and desorption branches yielded coefficients of determination (R2) of 0,995 and 0,992, for both desorption and adsorption, respectively. This indicates a high degree of linearity and repeatability. From the slope of the frequency-humidity calibration curves, the sensor's sensitivity parameter (S) can be extracted. It quantifies the variation of the resonance frequency in response to relative humidity (RH) changes, as expressed in the *equation* 6 [45]. The limit of detection (LOD), however, which indicates the capability of the sensor to detect very small humidity variations with high precision, can be calculated according to *equation* 7.

$$S = \frac{\Delta f_r}{\Delta_{RH} \times f_r^0} \times 10^6 \left(\frac{\text{ppm}}{\%\ \text{RH}} \right) \tag{6}$$

$$LOD = \left(3 \times \frac{f_{STDEV}}{Sensitivity} \right) (\%\ RH) \tag{7}$$

The calculated sensitivity of the SAW sensor exhibits an interesting value of -16.8 ppm/ %RH, which compares favorably with those reported in the literature [46] [47] [10] [48] [49] (see Table S1 in supplementary information). Furthermore, while the limit of detection (LOD) is 0.3%RH, confirming the capability of our sensor to detect very small humidity variations with high precision.

Based on what have proceeded, it is observed that the sensor exhibits high sensitivity with excellent linearity, along with a reasonable response and recovery time during both adsorption desorption cycles. This is owing to the selectively tuned properties of the PEDOT:PSS layer, enabling its uniformity and controlled roughness, ensuring strong adhesion to the gold electrodes and stable transduction of humidity-induced signals. Although the sensing dynamics are influenced by the gradual diffusion of water molecules within the polymer matrix, the electrochemically deposited PEDOT:PSS film provides enhanced reproducibility compared with conventionally coated layers. Owing to these advantages, the developed sensor is well suited for applications in, industrial process control, healthcare, and smart detecting systems.

IV.CONCLUSION

In this paper, a shear-horizontal surface acoustic wave (SH-SAW) resonator was designed and characterized for humidity sensing applications. The active sensing layer, based on PEDOT:PSS conducting polymer, was grown directly on top of interdigital transducers (IDTs) by means of electrochemical deposition, a technique that enables precise control over the film's thickness, uniformity, and morphology. The fabricated sensor exhibits a stable and repeatable response over the tested humidity range, with a measurable downshift in resonance

frequency due to the combined mass loading and dielectric modulation effects induced by water adsorption on the PEDOT:PSS layer. The electrical behavior of the resonator was modeled using the modified Butterworth–Van Dyke (mBVD) equivalent circuit, showing excellent agreement with the experimental S_{11} measurements. The developed device exhibited a sensitivity of -16.8 ppm/%RH and a limit of detection (LOD) of 0.3%RH, demonstrating competitive performance compared with state-of-the-art SAW-based humidity sensors. These results highlight the advantages of the controlled electrochemical deposition process, confirming its potential for fabricating high-performance, reliable, and miniaturized SAW humidity sensors suitable for environmental, industrial, and biomedical monitoring applications.

ACKNOWLEDGMENT

Author Contributions: B.H. conceived of the project. B.H. and A.W. designed and conducted the experiments. O.S, B.H and A.W conducted the theoretical study for the BVD model. A.W. conducted M-BVD equivalent circuit simulations, characterization and data analysis. AW, N.A conducted the chemical aspect: EDOT:PSS solution preparation, Electrochemical deposition and data analysis. AW, P.D and M.L conducted the Nextron setup for Humidity measurements. B.H, AW and N.A wrote the paper. All authors have read and agreed to publish this version of the manuscript.

Funding: The authors gratefully acknowledge financial support from the Hauts-de-France region, the CNRS' through the "STIMulE-STIP" call for projects (contract no. 272894, COSMOS^2, UMR 8520) and the French National Nanofabrication Network RENATECH for micro and nanofabrication.

Special thanks to Melanie Brouillard for the help during the SAW sensors' fabrication process.

Conflicts of Interest: The authors declare no conflict of interest.

Data Availability: All data supporting this study are openly available in a GitHub link:

https://github.com/Bilel-HAFSI/SNIFFER.git

REFERENCE

[1] G. Wang *et al.*, « Fast-response humidity sensor based on laser printing for respiration monitoring », *RSC Adv.*, vol. 10, nº 15, p. 8910-8916, 2020, doi: 10.1039/C9RA10409G.
[2] « B. Wang, M. K. Law and A. Bermak, "A low-cost capacitive relative humidity sensor for food moisture monitoring application," 2012 4th Asia Symposium on Quality Electronic Design (ASQED), Penang, Malaysia, 2012, pp. 95-99, doi: 10.1109/ACQED.2012.6320483. »
[3] « Bridgeman, D.; Corral, J.; Quach, A.; Xian, X.; Forzani, E. Colorimetric Humidity Sensor Based on Liquid Composite Materials for the Monitoring of Food and Pharmaceuticals. Langmuir 2014, 30, 10785–10791. »
[4] A. Lokman, H. Arof, S. W. Harun, Z. Harith, H. A. Rafaie, et R. M. Nor, « Optical Fiber Relative Humidity Sensor Based on Inline Mach–Zehnder Interferometer With ZnO Nanowires Coating », *IEEE Sensors J.*, vol. 16, nº 2, p. 312-316, janv. 2016, doi: 10.1109/JSEN.2015.2431716.
[5] X. Zhang *et al.*, « Printed Carbon Nanotubes-Based Flexible Resistive Humidity Sensor », *IEEE Sensors J.*, vol. 20, nº 21, p. 12592-12601, nov. 2020, doi: 10.1109/JSEN.2020.3002951.
[6] N. Li, X.-D. Chen, X.-P. Chen, X. Ding, et X. Zhao, « Ultra-High Sensitivity Humidity Sensor Based on MoS_2 /Ag Composite Films », *IEEE Electron Device Lett.*, vol. 38, nº 6, p. 806-809, juin 2017, doi: 10.1109/LED.2017.2699332.
[7] X. Le *et al.*, « Surface acoustic wave humidity sensors based on uniform and thickness controllable graphene oxide thin films formed by surface tension », *Microsyst Nanoeng*, vol. 5, nº 1, p. 36, juill. 2019, doi: 10.1038/s41378-019-0075-0.
[8] Y. Dou *et al.*, « Surface acoustic wave relative humidity sensor based on GO/TiO2 sensitive film », *Sensors and Actuators A: Physical*, vol. 365, p. 114906, janv. 2024, doi: 10.1016/j.sna.2023.114906.
[9] Y. Tang *et al.*, « Highly sensitive surface acoustic wave (SAW) humidity sensors based on sol–gel SiO2 films: Investigations on the sensing property and mechanism », *Sensors and Actuators B: Chemical*, vol. 215, p. 283-291, août 2015, doi: 10.1016/j.snb.2015.03.069.
[10] S. I. Jung, I. R. Jang, C. Ryu, J. Park, A. M. Padhan, et H. J. Kim, « Graphene oxide decorated multi-frequency surface acoustic wave humidity sensor for hygienic applications », *Sci Rep*, vol. 13, nº 1, p. 6838, avr. 2023, doi: 10.1038/s41598-023-34099-7.
[11] T. A. Blank, L. P. Eksperiandova, et K. N. Belikov, « Recent trends of ceramic humidity sensors development: A review », *Sensors and Actuators B: Chemical*, vol. 228, p. 416-442, juin 2016, doi: 10.1016/j.snb.2016.01.015.
[12] W. F. Yanto *et al.*, « Humidity sensors based on doped ZnO: An overview », *Materials Today: Proceedings*, p. S2214785324001755, mars 2024, doi: 10.1016/j.matpr.2024.03.049.
[13] H. Ma *et al.*, « Recent Advances in Graphene-Based Humidity Sensors With the Focus on Structural Design: A Review », *IEEE Sensors J.*, vol. 24, nº 13, p. 20289-20311, juill. 2024, doi: 10.1109/JSEN.2024.3398003.
[14] Y. T. Ravikiran et B. Chethan, « Humidity sensing studies on conducting polymers: Polyaniline and polypyrrole », *Inorganic Chemistry Communications*, vol. 145, p. 110019, nov. 2022, doi: 10.1016/j.inoche.2022.110019.
[15] « Assunção da Silva, E., Duc, C., Redon, N. and Wojkiewicz, J.-L. (2021), Humidity Sensor Based on PEO/PEDOT:PSS Blends for Breath Monitoring. Macromol. Mater. Eng., 306: 2100489. https://doi.org/10.1002/mame.202100489 ».
[16] L. Bießmann, L. P. Kreuzer, T. Widmann, N. Hohn, J.-F. Moulin, et P. Müller-Buschbaum, « Monitoring the Swelling Behavior of PEDOT:PSS Electrodes under High Humidity Conditions », *ACS Appl. Mater. Interfaces*, vol. 10, nº 11, p. 9865-9872, mars 2018, doi: 10.1021/acsami.8b00446.
[17] L. Zhanshayeva, V. Favaron, et G. Lubineau, « Macroscopic Modeling of Water Uptake Behavior of PEDOT:PSS Films », *ACS Omega*, vol. 4, nº 26, p. 21883-21890, déc. 2019, doi: 10.1021/acsomega.9b02866.
[18] « Romero, F.J.; Rivadeneyra, A.; Becherer, M.; Morales, D.P.; Rodríguez, N. Fabrication and Characterization of Humidity Sensors Based on Graphene Oxide–PEDOT:PSS Composites on a Flexible Substrate. Micromachines 2020, 11, 148. https://doi.org/10.3390/mi11020148 ».
[19] G. Hassan, M. Sajid, et C. Choi, « Highly Sensitive and Full Range Detectable Humidity Sensor using PEDOT:PSS, Methyl Red and Graphene Oxide Materials », *Scientific Reports*, vol. 9, nº 1, p. 15227, oct. 2019, doi: 10.1038/s41598-019-51712-w.
[20] « Popov, Vasiliy I et al. "Graphene-PEDOT: PSS Humidity Sensors for High Sensitive, Low-Cost, Highly-Reliable, Flexible, and Printed Electronics." Materials (Basel, Switzerland) vol. 12,21 3477. 24 Oct. 2019, doi:10.3390/ma12213477 ».
[21] G. Sasikanth, B. V. R. S. Subramanyam, et T. P. Radhakrishnan, « Efficient Humidity Sensing and Stable Moisture Energy Generation with Polyaniline Emeraldine Base – Poly(sodium 4-styrenesulfonate) Thin Film », *J. Phys. Chem. C*, vol. 128, nº 26, p. 10818-10825, juill. 2024, doi: 10.1021/acs.jpcc.4c02578.
[22] M. F. De Aguiar, A. N. R. Leal, C. P. De Melo, et K. G. B. Alves, « Polypyrrole-coated electrospun polystyrene films as humidity sensors », *Talanta*, vol. 234, p. 122636, nov. 2021, doi: 10.1016/j.talanta.2021.122636.
[23] L. Routier *et al.*, « Single-point calibration process based integrated electrical impedance analyzer for multi-selective gas detection », *Discov Appl Sci*, vol. 6, nº 8, p. 403, juill. 2024, doi: 10.1007/s42452-024-06102-x.
[24] I. Basak *et al.*, « Inkjet Printing of PEDOT:PSS Based Conductive Patterns for 3D Forming Applications », *Polymers*, vol. 12, nº 12, p. 2915, déc. 2020, doi: 10.3390/polym12122915.
[25] Y. Liu, X.-C. Sun, C. Lv, et H. Xia, « Green nanoarchitectonics with PEDOT:PSS–gelatin composite for moisture-responsive actuator and generator », *Smart Materials and Structures*, vol. 30, nº 12, p. 125014, nov. 2021, doi: 10.1088/1361-665X/ac31c6.
[26] B.-C. Shiu, Y.-L. Liu, Q.-Y. Yuan, C.-W. Lou, et J.-H. Lin, « Preparation and Characterization of PEDOT:PSS/TiO2 Micro/Nanofiber-Based Gas Sensors », *Polymers*, vol. 14, nº 9, 2022, doi: 10.3390/polym14091780.
[27] T. Julian, A. Rianjanu, S. N. Hidayat, A. Kusumaatmaja, R. Roto, et K. Triyana, « Quartz crystal microbalance coated with PEDOT–PSS/PVA nanofiber for a high-performance humidity sensor », *Journal of Sensors and Sensor Systems*, vol. 8, nº 2, p. 243-250, 2019, doi: 10.5194/jsss-8-243-2019.
[28] T. He *et al.*, « Beyond energy harvesting - multi-functional triboelectric nanosensors on a textile », *Nano Energy*, vol. 57, p. 338-352, mars 2019, doi: 10.1016/j.nanoen.2018.12.032.
[29] R. D. McCullough, « The Chemistry of Conducting Polythiophenes », *Advanced Materials*, vol. 10, nº 2, p. 93-116, janv. 1998, doi: 10.1002/(SICI)1521-4095(199801)10:2%3C93::AID-ADMA93%3E3.0.CO;2-F.
[30] Md. A. Khaleque, M. Aly Saad Aly, et Md. Z. H. Khan, « Chemical and electrochemical synthesis of doped conducting polymers and their application in supercapacitors: An overview », *Chemical Engineering Journal*, vol. 507, p. 160444, mars 2025, doi: 10.1016/j.cej.2025.160444.
[31] « Kabanova, V.; Gribkova, O.; Nekrasov, A. Poly(3,4-ethylenedioxythiophene) Electrosynthesis in the Presence of Mixtures of Flexible-Chain and Rigid-Chain Polyelectrolytes. Polymers 2021, 13, 3866. https://doi.org/10.3390/polym13223866 ».
[32] D. R. Santos, J. F. Zeferino, A. S. Viana, K. G. U. Wijayantha, K. Lobato, et J. P. Correia, « Temperature-dependent electrosynthesis of PEDOT:PSS: Enhanced Na+ transfer targeting high-performance Na-ion batteries ».
[33] F.-F. Pang, S. Li, W.-Q. Sun, et G.-Z. Han, « Reversible conductivity modulation of PEDOT:PSS based on pH », *Materials Chemistry and Physics*, vol. 186, p. 246-250, janv. 2017, doi: 10.1016/j.matchemphys.2016.10.050.
[34] E. Poverenov, M. Li, A. Bitler, et M. Bendikov, « Major Effect of Electropolymerization Solvent on Morphology and Electrochromic Properties of PEDOT Films », *Chem. Mater.*, vol. 22, nº 13, p. 4019-4025, juill. 2010, doi: 10.1021/cm100561d.
[35] A. Westrelin *et al.*, « Design and Fabrication Of Multiplexed One-Port SAW Resonators On A Single Chip ».
[36] L. Shen, W. Feng, D. Yu, et W. Wang, « High sensitive humidity sensor based on PEDOT:PSS/CMC-Na coated polyester fabric with directional moisture transport

performance », *Colloids and Surfaces A: Physicochemical and Engineering Aspects*, vol. 682, p. 132880, févr. 2024, doi: 10.1016/j.colsurfa.2023.132880.
[37] Vinita, D. Pareek, S. Kumar Gupta, et J. Singh, « Graphene Decorated Shear Horizontal Surface Acoustic Wave Resonator as Humidity Sensor », *IEEE Sensors J.*, vol. 24, nº 20, p. 31932-31939, oct. 2024, doi: 10.1109/JSEN.2024.3447069.
[38] S. S. Kalagi et P. S. Patil, « Secondary electrochemical doping level effects on polaron and bipolaron bands evolution and interband transition energy from absorbance spectra of PEDOT: PSS thin films », *Synthetic Metals*, vol. 220, p. 661-666, oct. 2016, doi: 10.1016/j.synthmet.2016.08.009.
[39] M. Zhu *et al.*, « Simple approach for the fabrication of PEDOT-coated Si nanowires », *Beilstein J. Nanotechnol.*, vol. 6, p. 640-650, 2015, doi: 10.3762/bjnano.6.65.
[40] B. Lu *et al.*, « Pure PEDOT:PSS hydrogels », *Nature Communications*, vol. 10, nº 1, p. 1043, mars 2019, doi: 10.1038/s41467-019-09003-5.
[41] Q. Wei, M. Mukaida, K. Kirihara, Y. Naitoh, et T. Ishida, « Thermoelectric power enhancement of PEDOT:PSS in high-humidity conditions », *Applied Physics Express*, vol. 7, nº 3, p. 031601, févr. 2014, doi: 10.7567/APEX.7.031601.
[42] E. S. Muckley, C. B. Jacobs, R. Kumar, et I. N. Ivanov, « Effect of water adsorption on ionic and electronic transport in PEDOT:PSS (Conference Presentation) », in *Organic Sensors and Bioelectronics X*, R. Shinar, I. Kymissis, et L. Torsi, Éd., San Diego, United States: SPIE, sept. 2017, p. 25. doi: 10.1117/12.2274496.
[43] A. G. Guruge, H. Makki, et A. Troisi, « Structural properties of conductive polymer blends interfaced with water: computational insights from PEDOT:PSS », *J. Mater. Chem. C*, vol. 12, nº 47, p. 19245-19257, 2024, doi: 10.1039/D4TC03066D.
[44] « Saha, A.; Ohori, D.; Sasaki, T.; Itoh, K.; Oshima, R.; Samukawa, S. Effect of Film Morphology on Electrical Conductivity of PEDOT:PSS. Nanomaterials 2024, 14, 95. https://doi.org/10.3390/nano14010095 ».
[45] C. Li *et al.*, « Highly sensitive and fast response Love wave mode humidity sensor based on MoS2@Ti3C2Tx hierarchical structure », *Sensors and Actuators B: Chemical*, vol. 387, p. 133823, juill. 2023, doi: 10.1016/j.snb.2023.133823.
[46] A. Rianjanu *et al.*, « Quartz crystal microbalance humidity sensors integrated with hydrophilic polyethyleneimine-grafted polyacrylonitrile nanofibers », *Sensors and Actuators B: Chemical*, vol. 319, p. 128286, sept. 2020, doi: 10.1016/j.snb.2020.128286.
[47] « Chen, Q.; Liu, D.; Huang, X.-H.; Yao, Y.; Mao, K.-L. Impedance Analysis of Chitin Nanofibers Integrated Bulk Acoustic Wave Humidity Sensor with Asymmetric Electrode Configuration. Nanomaterials 2022, 12, 3035. https://doi.org/10.3390/nano12173035 ».
[48] C. Wang *et al.*, « Surface acoustic wave sensor based on Au/TiO2/PEDOT with dual response to carbon dioxide and humidity », *Analytica Chimica Acta*, vol. 1190, p. 339264, janv. 2022, doi: 10.1016/j.aca.2021.339264.
[49] C. Li *et al.*, « Highly sensitive and fast response Love wave mode humidity sensor based on MoS2@Ti3C2Tx hierarchical structure », *Sensors and Actuators B: Chemical*, vol. 387, p. 133823, juill. 2023, doi: 10.1016/j.snb.2023.133823.

Authors

Nour Abdallah is currently a Master 2 student in chemistry at the University of Lille, France. She is completing her master's internship at ICAM School of Engineering in Lille, working on the SNIFFER project. This research focuses on the development of a connected and autonomous sensing platform based on Surface Acoustic Wave (SAW) sensors for multivariate detection of complex gas mixtures. Her interests include sensor technology, gas detection systems, and embedded electronics for environmental and health monitoring applications.

Alexandre WESTRELIN recently graduated from the ICAM engineering school in Lille. He holds an engineering degree specializing in the fields of transport, logistics, and energy. During his studies in 2022, Alexandre actively participated in a research memoir focused on applied material science. His research involved the design and development of an integrated platform for the characterization of SAWs (Surface Acoustic Wave) sensors. This project showcased his expertise and interest in cutting-edge technologies. Currently, Alexandre is employed at "MC2 Technologies," a prominent company based in Villeneuve d'Ascq. The company specializes in the development of advanced RF microwave-based protection systems. Within MC2 Technologies, Alexandre serves as an automation engineer, responsible for system installation and testing. His role involves ensuring the smooth integration and functionality of the company's cutting-edge systems.

Pierre Debavelaere is an apprentice student at ICAM school engineering ICAM, Lille, France. As part of his final year, he conducted a six-month research project between September 2024 and mid-February 2025, under the supervision of Dr. Bilel Hafsi. This project focused on the characterization of SAW sensors for gas detection. Pierre is currently working at SNCF (French National Railway Company) as part of the department focused on the evolution and modernization of test systems. His work involves the development and integration of innovative testing methods and tools to support maintenance and reliability operations within the railway sector.

Mathieu Lefebvre is an apprentice student at ICAM school engineering, Lille, France. As part of his final year, he conducted a six-month research project between September 2024 and mid-February 2025, under the supervision of Dr. Bilel Hafsi. This project focused on the characterization of SAW sensors for gas detection. The main objective of the project was the installation and implementation of a test bench enabling precise evaluation of sensor performance under controlled environmental conditions. In parallel with this project, Mathieu Lefebvre is currently working as a project manager apprentice at Framatome a French multinational company specializing in the design, construction, and maintenance of nuclear power plants and components.

Dr. Olivier Stienne received the engineering degree in electronics engineering from the CNAM Engineering School, Paris, France, in 1999. Obtained his Ph.D. degree in micro and nanotechnologies, acoustic, and telecommunications within the Interference and Electromagnetic Compatibility Group, Lille University, Villeneuve d'Ascq, France. He worked for 10 years in the industry. Then, he joined the E.E.A. Department, Icam, Lille, where he teaches electronics and telecommunications to engineering students. His current research interests include the analysis of the impact of electromagnetic interference on the performance of wireless communication using orthogonal frequency division multiplexing modulation.

Dr. Bilel HAFSI received the master's degree in materials, nanostructures, devices et microelectronics systems from Monastir University, Tunisia, in 2012 and the PhD. degree in micro et nanoelectronics, acoustic and telecommunications from Lile University, France, in 2016. From 2016 to 2018, he was a Teacher and Research Assistant with the central Lille institute. His research interest includes the development of Devices based organic materials, and fabrication of micro- or nanostructured surfaces. To expand these concepts, he focused on developing new kind of memory devices based on double floating gate made of gold nanoparticles and reduced graphene oxide. his main interest was to boost the memory performance (endurance, memory window and retention time). From 2018 to 2019 he has experienced the Job of a Dream consultant in private company "Techshop Les Ateliers Leroy Merlin" where he supervised many projects in the field of IOT's, Robotics ...Currently, he works as associate professor in the electrical department in ICAM school of engineering, Lille 59800, France. Dr. Bilel HAFSI was a recipient of the International research Young Scientist Award in 2018 from the doctoral college in the north of France.